15th IFK
Proc. of the 15th International Fluid Power Conference <Symposium/Conference>
<DOI>

Enhancing Volumetric Efficiency and Productivity of External Gear Pumps through Optimized Run-In Strategies.

Alfonso Rosario Apuzzo[1*,2], Sara Bonati[2], Emma Frosina[1] and Luca Riccò[2]

[1]*Department of Engineering, University of Sannio, Piazza Guerrazzi, 82100 Benevento, Italy.*

[2]*Duplomatic MS S.p.a., Via Mario Re Deapolini, 24, 20015, Parabiago Milan, Italy.*

** E-mail: a.apuzzo@studenti.unisannio.it*

Abstract.

In the final stage of production, External Gear Pumps (EGPs) must be run-in following a specific working cycle in which the pump body is subject to material removal resulting in a consequent increase in energy demand. The run-in cycle impacts the pump performance and the production costs. In this study, five new run-in cycles are defined with the objective to analyse the impact on the power absorbed during and after the cycle, the material removed from the body and the impact on pump performance. The work shows that the use of different run-in cycles can result in a higher pump volumetric efficiency, up to + 2%, combined with a cost reduction of 1.74% and an increase of productivity of 78%. Subsequently, experimental data were used to define a preliminary AI based algorithm to predict the run-in cycles parameter. The AI algorithm, which was trained and validated on the experimental data, demonstrated a high predictive capability with a maximum error of 6%.

Keywords. External Gear Pump, Run-in cycle, Efficiency, AI Algorithms.

1. INTRODUCTION

External Gear Pumps (EGPs) are positive displacement machines widely used in fluid power applications across both mobile and industrial sectors. EGPs are widely chosen, having a good combination of performance, reliability and cost-effectiveness. The EGP under study, manufactured by Hydreco (HY2.16 pump), is a fixed positive displacement machine of 16 cm^3/rev capable of operating at a maximum pressure of 260 bar and a rotational speed range of 500 – 3200 rpm. It finds application in a wide range of fields, from agriculture to material handling and aeronautics devices. In Figure 1. 1, an exploded view of HY2.16, a pressure compensated (PC) EGP, is shown.

Before being delivered to customers, EGP is end-of-line (EoL) tested with a specific run-in cycle in which the pressure forces cause the gears translation and inflection towards the suction side. In this condition, the tips of gears' teeth interfere with the pump body. Due to these micro-movements of the gears, typically made of hardened steel, the body on the low-pressure side undergoes a milling phase. The gears dig their optimal seats into the body and, as a result, leakage flows can be minimized (maximization of the volumetric efficiency) at that operating condition.

The run-in cycle has a relevant importance for EGPs, as it defines the internal profile of the pump housing (or body) and, consequently, its efficiency. This cycle is usually performed at a constant speed within the operative pump range, but different levels of speed can be adopted [1, 2].

Figure 1. 1– Exploded view of Hydreco HY2 pump (aluminium housing)

The amount of removed material is related to the operative working conditions and the clearance variability [1]. Once the material removal phase is complete, a performance check (testing) phase is conducted to verify the pump's performance. The duration time of the cycle depends on the pump tested, it can vary from a couple of minutes [1] until to 15 minutes [3]. This time impacts on the total cost of an EGP which is given by the summation of the components, assembly and EoL testing (run-in and performance check) costs. Specifically, the assembly and EoL testing costs are strictly dependent on the hourly operating cost, which typically ranges between the 30 – 60€/h.

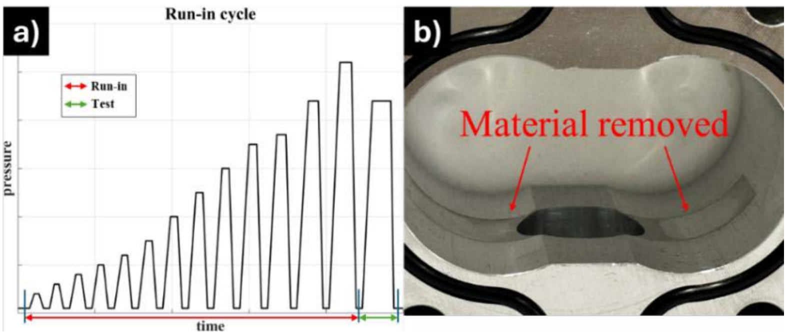

Figure 1. 2 – a) Standard run-in cycle; b) Gear seats with removed material after the run-in cycle.

Figure 1. 2.a shows an example of a typical run-in cycle in which the load pressure has a step variation; the run-in and testing phase are highlighted. Figure 1. 2.b shows how the gear seats appear after the cycle in Figure 1. 2.a.

In the open literature, there are only a limited number of studies focused on the run-in cycles and correlated effects on the pump performance. The first work was published by M. Borghi et al. [2]. The authors developed a simple analytic model to predict the internal profile of the pump body for different run-in pressures and rotational speeds. The gear position was defined by two contributions, the recovery of radial clearances, as in [4] and the eccentricity contribute evaluated with the Sommerfield theory. In [2], the impact for different run-in speeds in range 500 – 3000 rpm was presented. In [2] and [4], the calculation of the internal body profile is integrated into lumped-parameter models, thus enabling the correlation of post-run-in geometrical variations with the unit performance. In [1], a lumped parameter model for EGPs was adapted to predict the run-in cycle and the amount of material removed was calculated in each pressure step. The authors verified experimentally and numerically that the major amount of material was removed in the first low pressure ramps, and they proposed a shorter cycle removing four out of thirteen ramps at the middle-hight pressures and extending two ramps at low pressures. In [3], the authors proposed a mathematical model for EGPs that can predict the volume of material removed under different operating conditions and define a run-in cycle for applications up to 400 bar. The proposed cycle has been defined to have the same depth of asportation for each pressure ramp. In these studies, the authors refer to cycles with a standard shape as reported in Figure 1. 2.a. and no references to different shapes are present. More recently, there has been an ever-increasing diffusion and interest in the AI algorithms, including their application in the study of EGPs. In [5] neural networks were used to predict the output flow-rate of an EGP, while in [6], machine learning algorithms were used for predictive maintenance. However, based on the best knowledge, studies using AI algorithms to investigate the run-in cycle on EGPs are not present in the open literature.

In the present work, starting from a baseline run-in cycle, used as a reference, and the authors' expertise, five new cycles have been defined. A sample of thirty EGPs was tested and for each pump, its performance characterization was performed to evaluate in detail the impact of the new run-in cycles. In addition, torque and pressure have been acquired during the run-in cycle to estimate the absorbed energy and to identify the phases in which the material removal occurs. Moreover, the wear profile on the gear seats was measured using a 3D Coordinate Measuring Machine (CMM). Finally, a preliminary model based on AI algorithm has been developed. The acquired experimental data were used in part to train AI algorithm and in part to test it, showing a very good alignment.

The aim of the present work is to define new run-in cycles that allow to have a shorter test time and to preserve and improve the pump performance. Cycles with an innovative pressure shape which differ from [1, 3] will be presented and analysed.

2. Experimental Activity – Run-in Cycles and Pumps Definition

Five new run-in cycles, with a shorter time duration, were defined to reduce both the pump cost and energy consumption to have as resulting also economic and environmental benefits. For each cycle, five pumps have been properly assembled and tested.

2.1. *Run-in cycles*

The run-in cycle is defined as a load cycle performed at a specified rotational speed (N), which can be either constant or variable over time. The term load cycle refers to the evolution of pressure over time. In this work six run-in cycles have been defined through five different load cycles that can be grouped in three different families identified as A, B and C. Table 2. 1 summarises the parameters that define each cycle.

A	B	C
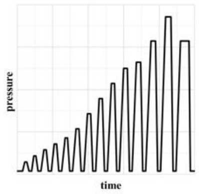	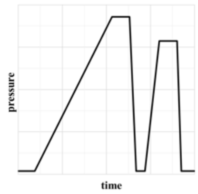	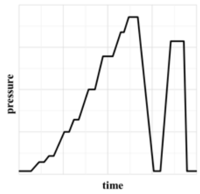
$\# \boldsymbol{S}\, ; \boldsymbol{p_i^{max}}\, ; \boldsymbol{t_i^j}\, ; \boldsymbol{p_{test}}\, ;\ \boldsymbol{t_{test}}$	$\boldsymbol{p^{max}}\, ; \boldsymbol{t^j}; \boldsymbol{p_{test}}\, ;\ \boldsymbol{t_{test}}$	$\# \boldsymbol{S}\, ; \boldsymbol{p_i^{max}}\, ; \boldsymbol{t_i^j}\, ; \boldsymbol{p_{test}}\, ;\ \boldsymbol{t_{test}}$
$i = 1, 2, \ldots, \# S$ $j = 1, 2, \ldots, 4$	$j = 1, 2, \ldots, 4$	$i = 1,2, \ldots, \# S$ $j = 1, 2, 3\ if\ i = 1, 2, \ldots, \# S - 1$ $j = 2, 3, 4\ if\ i = \# S$

Table 2. 1 – Load cycles definition

The variable $\# \boldsymbol{S}$ is the number of pressure steps, $\boldsymbol{p_i^{max}}$ the pressure of the i-th ramp and $\boldsymbol{t_i^j}$ one of the four times that define the ramp i-th. The times $\boldsymbol{t^j}$ used to define the pressure ramps are: 1) t^1 : time at low pressure; 2) t^2: time to pass from low to high pressure; 3) t^3 : time at high pressure; 4) t^4 : time to pass from high to low pressure. The parameters $\boldsymbol{t_{test}}$ and $\boldsymbol{p_{test}}$ define the test ramp that for this study has been maintained constant for all the cycles. Another common parameter for all the cycles is the $\boldsymbol{p_S^{max}}$, which value is the one used to run-in the pump for the maximum operative pressure. The defined run-in cycles are reported in the Table 2. 2. Although the actual values of these parameters are not disclosed for confidentiality reasons, it can be stated that $N_2 = 2 * N_1$, $S_{New} < S_{STA}$, $t_{1STEP\ 3}^2 = 4 * t_{1STEP\ 1}^2$ and the t_S^3 (time at maximum pressure) is the same for all cycles.

The last two columns of Table 2.2 show the percentage variations in the new cycles compared to the current reference, called STA N1.

Table 2. 2 - Run-in cycles defined

ID cycle	Load cycle	$\# \boldsymbol{S}$	$\boldsymbol{N_{Run-in}}$	$\boldsymbol{N_{test}}$	$\boldsymbol{t_{cycle}}$	$\boldsymbol{E_{cycle}}$
STA N1	*A*	S_{STA}	N_1	N_1	t_{STA}	E_{STA}
STA N2	*A*	S_{STA}	N_2	N_1	*+0.0%*	*+100%*
STAIR	*C*	S_{STA}	N_1	N_1	*-34.6%*	*-17.4%*
New STA	*A*	S_{New}	N_1	N_1	*-29.5%*	*-32.9%*
1STEP 1	*B*	*1*	N_1	N_1	*-57.4%*	*-49.3%*
1STEP 3	*B*	*1*	N_1	N_1	*-39.7%*	*-23.4%*

As shown in Table 2. 2, all new cycles, except for STA N2, are better than STA N1 in terms of cost reduction, thanks to their shorter duration and lower theoretical energy demand (equation 2.1).

$$E\ [J] = \int_{t=0}^{t_{cycle}} T_{th} * \omega * dt \tag{2. 1}$$

The new cycles, with a reduced run-in time compared to STA N1 provide an increment of the test rig productivity $\#Pumps/h$, defined as the number of pumps tested hour (Table 2. 3). It was considered constant the time to allocate the pump on the test rig as the cycle changes.

Table 2. 3 – Test rig productivity compared to the STA N1 cycle

	STA N2	STAIR	New STA	1STEP 1	1STEP 3
$\boldsymbol{\#Pumps/h}$	*+0.00%*	*+36.12%*	*+29.29%*	*+78.61%*	*+43.99%*

A shorter run-in time allows for reducing the production cost and finally, combined with the lower energy demand, impacts on the greenhouse gas emissions (GHG) due to the production process, an aspect not negligible considering the objective of a zero net GHG by 2050 established by the Daikin Group, of which Hydreco is a member.

2.2. Samples assembly

Five pumps have been tested for each run-in cycle. To avoid that experimental results could be influenced by the manufacturing capability, pumps have been assembled combining the components to keep basically constant the average radial clearance between gears and body $\boldsymbol{\delta_r^{av.}}$, and the maximum radial shift of the shafts $\epsilon_{max}^{av.}$. Five kits composed of two thrust plates, driven and driving gears were defined and kept constant. Consequently, thirty pump bodies have been selected, ensuring the smaller possible variability of radial interference $\boldsymbol{int}$. Refer to appendix for the definition of $\boldsymbol{\delta_r^{av.}}$, $\epsilon_{max}^{av.}$ and $\boldsymbol{int}$.

The relative standard deviation (RSD) of $\boldsymbol{int}$, defined as the ratio between the standard deviation and the mean value, was 4.6%. This corresponds to a value within the measurement accuracy of the CMM used for measuring the pump bodies (section 3.3), and it was considered acceptable. As concerns axial clearance, there was more variability, with an RSD of 24.6%; nevertheless, for the purposes of this study, this variability was considered not to impact and thus negligible.

2.3. Test bench layout

Figure 2. 1 shows the hydraulic scheme of the test bench used for the dynamic characterization of the run-in cycles and the acquisition of pump performances in steady-state conditions. During the run-in cycle were acquired the suction (1) and delivery (2) pressures, the torque (3) and the shaft speed (4). While the performance test also acquired the delivery flow rate (5).

Table 2. 4 - Sensors used for the experimental characterization

#ID	Symbol	Component	Range	Accuracy
1	p_1	Trafag 8845.73	0 - 1.6 barA	±0.5% of span
2	p_2	Trafag 8254.84	0 - 400 bar	±0.4% of span
3	T_{eff}	NCTE Series 3000-Model 250	0 - ±250 Nm	±0.2% of span
4	N	Rotary Encoder	0 - ±3000 r/min	±0.05% of span
5	Q_{eff}	Flow meter KRACHT - size 3	0 - 120 l/min	±0.3% of span

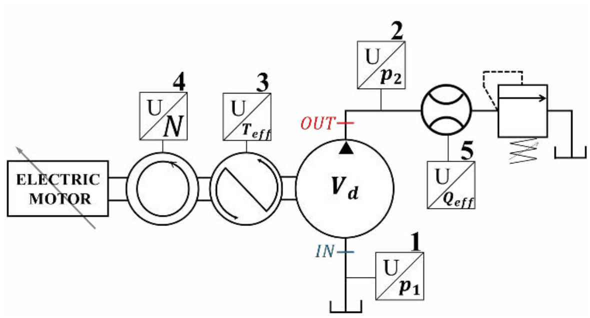

Figure 2. 1 - Test rig layout

The specifications of the used transducers are reported in Table 2. 4. For the dynamic acquisition of the run-in cycles, a sample frequency of 1kHz and a saving frequency of 20Hz were set. The steady state acquisition of the efficiencies, in the pressure range [60 - 240 bar] and in the speed range [1000 - 3000 rpm], has been performed with a sample and saving frequencies of 1kHz. An ISO VG-46 oil with a temperature setting of $39 \pm 2°C$ was used for the tests. The working operative point is varied by means the pressure control valve and the electric motor.

3. Experimental Results and Discussion

A complete characterization of the new run-in cycles was executed and their impacts on the pump performance were analysed. Three separate acquisitions have been performed: 1) Run-in cycle; 2) Performance characterization; 3) Measurement of the material removal.

3.1. Run-in cycles – Instantaneous torque

The continuous acquisition of all the variables of interest marked from 1 to 4 in Figure 2. 1 was performed for the entire run-in cycle. The total efficiency, defined as the product of the volumetric and hydromechanical efficiencies, was calculated during the constant pressure portion of the test phase; refer to the last ramps of Figure 3. 1.

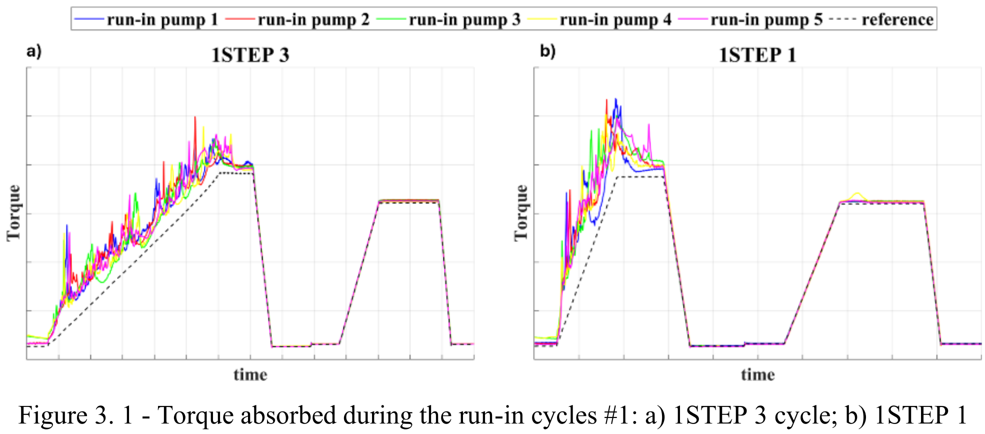

Figure 3. 1 - Torque absorbed during the run-in cycles #1: a) 1STEP 3 cycle; b) 1STEP 1 cycle. The scale factor of the time scale of graph "b" with respect to the graph "a" is 7:5.

Figure 3. 1 shows the torque during the run-in cycles of five pumps tested with 1STEP 1 and the 1STEP 3 run-in cycles (Table 2. 2). The black dashed line represents the torque absorbed when does no material removal occurs (after run-in is completed). It depends only on the pressure load and the pump mechanical losses, and it is identified as a reference curve. All the torque curves during the run-in phase show a higher mean value than the reference curves, as well as spikes and fluctuations due to interactions and contact between internal components during the material removal.

Table 3. 1 – Run-in cycles acquisition

ID cycle	$\boldsymbol{\delta E^{th}}$[%]	$\boldsymbol{\delta E^{eff}}$[%]	$\boldsymbol{E^{eff-mill}}$ [$\boldsymbol{kJ}$]	$\boldsymbol{T_{av}^{add}}$[$\boldsymbol{Nm}$]	$\boldsymbol{\delta T_{max}}$[%]
STA N1	*0%*	*0%*	*51.8*	*2.8*	*0%*
STA N2	*+100%*	*+81.4%*	*32.1*	*0.8*	*-13.8%*
STAIR	*-17.4%*	*-14.3%*	*49.4*	*4.0*	*-14.8%*
New STA	*-32.9%*	*-26.3%*	*48.3*	*3.6*	*-6.8%*
1STEP 1	*-49.3%*	*-45.7%*	*32.4*	*4.0*	*-7.8%*
1STEP 3	*-23.4%*	*-19.6%*	*54.2*	*4.7*	*-15.9%*

Table 3. 1 shows the average values of the most relevant physical quantities, calculated on the five pumps tested for each cycle. The first two columns show the percentage deviation from the reference cycle of the theoretical $\boldsymbol{E^{th}}$ and the effective $\boldsymbol{E^{eff}}$ energy required for the new cycles. The effective energy reduction (except for the cycle *STA N2)* of the new run-in cycles results smaller than the theoretical one. The relationship between $\boldsymbol{\delta E^{th}}$ and $\boldsymbol{\delta E^{eff}}$is described by equations (3. 1) and (3. 2); refer to the appendix for the simplifying assumptions adopted. Equation (3. 2) was obtained assuming that $\boldsymbol{E^{eff-mill}}$ (energy difference between the run-in cycles with and without material removal) is constant, however, experimental results have demonstrated that this is only true for four out of six cycles. The $\boldsymbol{E^{eff-mill}}$ required by the New STA and 1STEP 1 cycle is generally lower than that required by the other cycles. When $\boldsymbol{E^{eff-mill}}$ is not constant, equation (3. 2) becomes equation (3. 3).

$$\delta E_{i,j}^{eff}[\%] = \frac{\left(E_{i,j}^{eff-runin}+E_{i,j}^{eff-mill}\right)-\left(E_{STA\,N1,j}^{eff-runin}+E_{STA\,N1,j}^{eff-mill}\right)}{\left(E_{STA\,N1,j}^{eff-runin}+E_{STA\,N1,j}^{eff-mill}\right)}*100 \qquad (3.\ 1)$$

With $i = \{STA\ N1, STA\ N2, STAIR, New\ STA, 1STEP\ 1, 1STEP\ 3\}$; $j = 1,2,\ldots,5$

$$\delta E_{i,j}^{eff}[\%] = \delta E_i^{th} * A \quad ; \ 0 < A < 1 \qquad (3.\ 2)$$

$$\delta E_{i,j}^{eff}[\%] = \delta E_i^{th} * A + B \ ; \ 0 < A < 1 \qquad (3.\ 3)$$

The parameter $\boldsymbol{T_{av}^{add}}$ represents the average additional torque required by the pump during the cycle. It is defined by equation (3. 4).

$$T_{av}^{add} = \frac{1}{t_{cycle}}\int_{t=0}^{t_{cycle}}\left[T_{Run-in\,1}^{eff}(t) - T_{Run-in\,6}^{eff}(t)\right]*dt \qquad (3.\ 4)$$

In the last column of Table 3. 1, the maximum torque values obtained in the selected cycles are reported. The data show that the maximum torque in the new cycles is lower than that of the reference cycle.

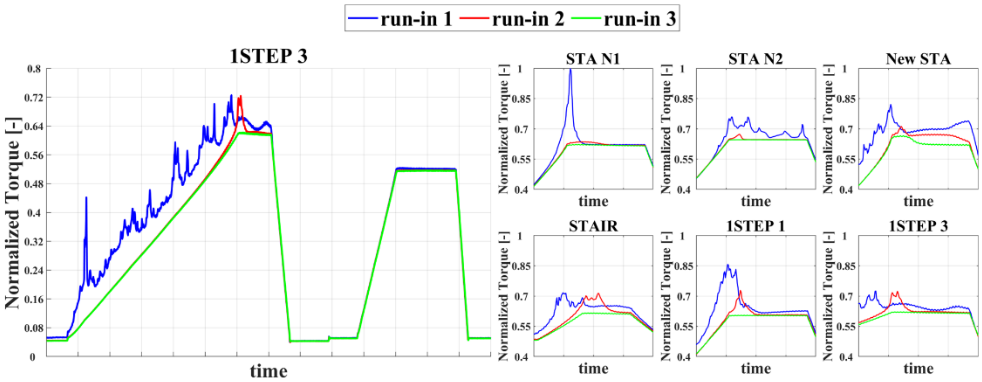

Figure 3. 2 - Torque absorbed by the 1STEP 3 run-in cycles 1, 2 and 3 of pump 1 with a zoomed view of the area at constant pressure of all the cycles.

The trend of $\boldsymbol{T_{av}^{add}}$ in Table 3. 1 is also confirmed in Figure 3. 2 in which the torque scales are normalized to the maximum torque of the STA N1 run-in 1. The left-hand side chart shows three consecutive run-in cycles of one pump during 1STEP 3 cycle. On the right-hand side, zoomed views of the area at the maximum constant pressure for all the six cycles are shown. It should be noted that the temporal extension shown is the same for all the zoomed views. Torque spikes were observed during the second and third consecutive run-in cycles for all tests except for STA N1. This seems to indicate that the material removal process was incomplete after the first run-in, suggesting that the selected $\boldsymbol{t_S^3}$ value was not optimal. Since, typically during the testing, the run-in cycle is performed only one time, it must be ensured that a complete material removal is obtained. Consequently, future run-in cycles will be designed with an increased value of $\boldsymbol{t_S^3}$ to be aligned to the actual one (STA N1).

For the EGP under investigation, the run-in phase (baseline cycle) represents the 3.95% of the production cost composed of: components, assembly phase and run-in cycle costs. In addition, the reduction of the run-in time allows not only to increase productivity (Table 2. 3) but, combined with a minor energy demand (Table 3. 1), allows for further reduction of the costs up to 1.74% (Table 3. 2).

Table 3. 2 – Pump cost compared to the STA N1 cycle

	STA N2	STAIR	New STA	1STEP 1	1STEP 3
Pump cost	*+0.03%*	*-1.04%*	*-0.90%*	*-1.74%*	*-1.20%*

Table 3. 2 shows as the major cost reduction is related to the reduction of the run-in time, in fact for STA N2 cycle a +81.4% of energy demand (Table 3. 1)corresponds to only +0.03% of the pump cost. In the present work, an energy cost of 0.12€/kWh was considered. Figure 3. 3 shows the efficiency values of each pump at the end of the run-in cycles. These efficiencies, referred to as the check operative point defined by the test phase, exhibit variation across different run-in cycles. The new run-in cycles seem to improve the pump performances; the benefit of the new run-in cycles is mainly impacting the volumetric efficiency that reaches values up to +1.5% respect to the one obtained with the standard run-in cycle.

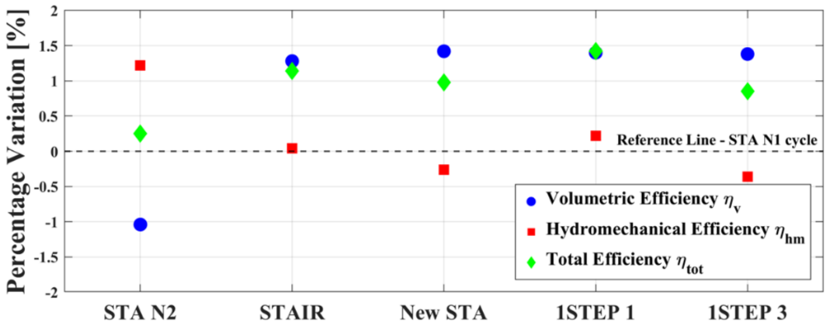

Figure 3. 3 - Run-in 1 efficiencies

3.2. Pump efficiencies

To confirm the results shown in the Figure 3. 3 a complete characterization of the pump efficiencies, acquiring #21 operative points, was performed. The characterization was carried out after repeated run-in, therefore the material removal phase can be considered complete for all bodies. The results pointed out nonsignificant variation for the hydromechanical efficiency (η_{hm}) while a more significant variation for the volumetric efficiency (η_v). Thus, Figure 3. 4 reports only the values of η_v in the different operating points.

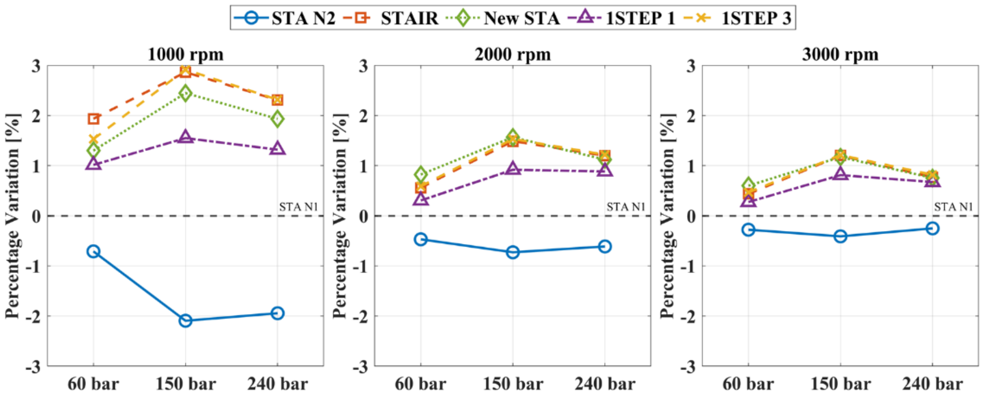

Figure 3. 4 - Volumetric Efficiency

The results show an effective improvement in volumetric efficiency for all cycles except STA N2, confirming the trend reported in Figure 3.3. The cycles defined in Table 2. 2 differ in shape, cycle time, and pump speed. The p_S^{max} value was the same for all the run-in cycles, but a reduction in cycle time corresponds to an increased pressure gradient. From the analysis of the volumetric efficiencies, it is possible state the following: 1) with fixed pressure gradient, an increase in run-in speed negatively impacts volumetric efficiency of the pump (STA N2 compared to STA N1); 2) with fixed run-in speed, an increased pressure gradient positively affects volumetric efficiency (STAIR, New STA, 1STEP 1 and 3 compared to STA N1). However, this effect reduces with excessive cycle time reduction (1STEP 1 compared to 1STEP 3); 3) with a fixed pressure gradient and rotational speed, a change of the cycle profile does not seem to have an impact on the volumetric efficiency

(STAIR compared to 1STEP 3). Cycles STAIR and 1STEP 3 have comparable cycle times and therefore comparable pressure gradients.

Regarding the cost reduction, the run-in cycle 1STEP 1, that is the shortest one, represents the optimal solution. However, considering the results reported in Figure 3. 4 the cycles 1STEP 3 and STAIR represent the best choices.

3.3. Measurement of the pump bodies

A CMM with an accuracy of 2 μm has been used to measure material removal. Results are presented in Figure 3. 5 and Table 3. 3, where the internal profiles measured in the central section of the pump body are reported.

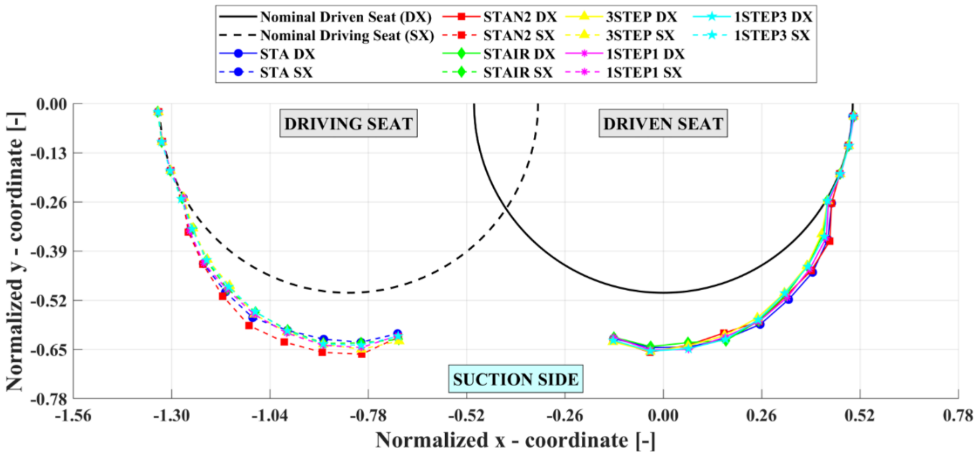

Figure 3. 5 - Measured material milled on the Internal pump body. DX identifies the driven gear while SX the driving one.

For confidential reasons, in Figure 3. 5 the axes are normalized to the tip diameter. The measured profiles differ slightly, with a maximum volume variation of 6%. The measured profile of the bodies run-in with cycle STA N2 shows a volume of material removed on the driving gear side comparable with the driven gear side (δV_{DX-SX}^{mill} below 4%). This can be directly correlated to the observed reduction of the volumetric efficiency (Figure 3. 4).

Table 3. 3 - Volume of material milled

	STA N1	STA N2	STAIR	New STA	1STEP 1	1STEP 3
$\boldsymbol{V_{DX}^{mill} + V_{SX}^{mill}}$	$V_{STA\,N1}^{mill}$	+5.94%	- 6.12%	-5.93%	-1.99%	-5.44%
$\boldsymbol{\delta V_{DX-SX}^{mill}}$	-15.82%	-3.82%	-16.56%	-13.93%	-16.53%	-17.43%

The use of a CMM permitted to obtain a 3D map of the milled regions, as showed in Figure 3. 6, and to estimate the volume of removed material (as reported in Table 3. 3). Figure 3. 6 and Figure 3. 7 show the 2D shape of the milled areas along the axial direction parallel to the rotation axis of gears and the 3D maps for the run-in cycles STA N2 and STAIR. For confidential reasons, the z-axes in Figure 3. 6 and Figure 3. 7 are normalized to the pump width. As previously observed in Figure 3. 5, for the STA N2 run-in cycle the depth of milling for the driving and driven gears seats are aligned. While for the STAIR run-in cycle the milling depth of the driven gear side is deeper than the one on the driving side.

Comparing the two cycles, a greater height of milling is observable for the STA N2 cycle with respect to the STAIR one, which returns a better volumetric efficiency.

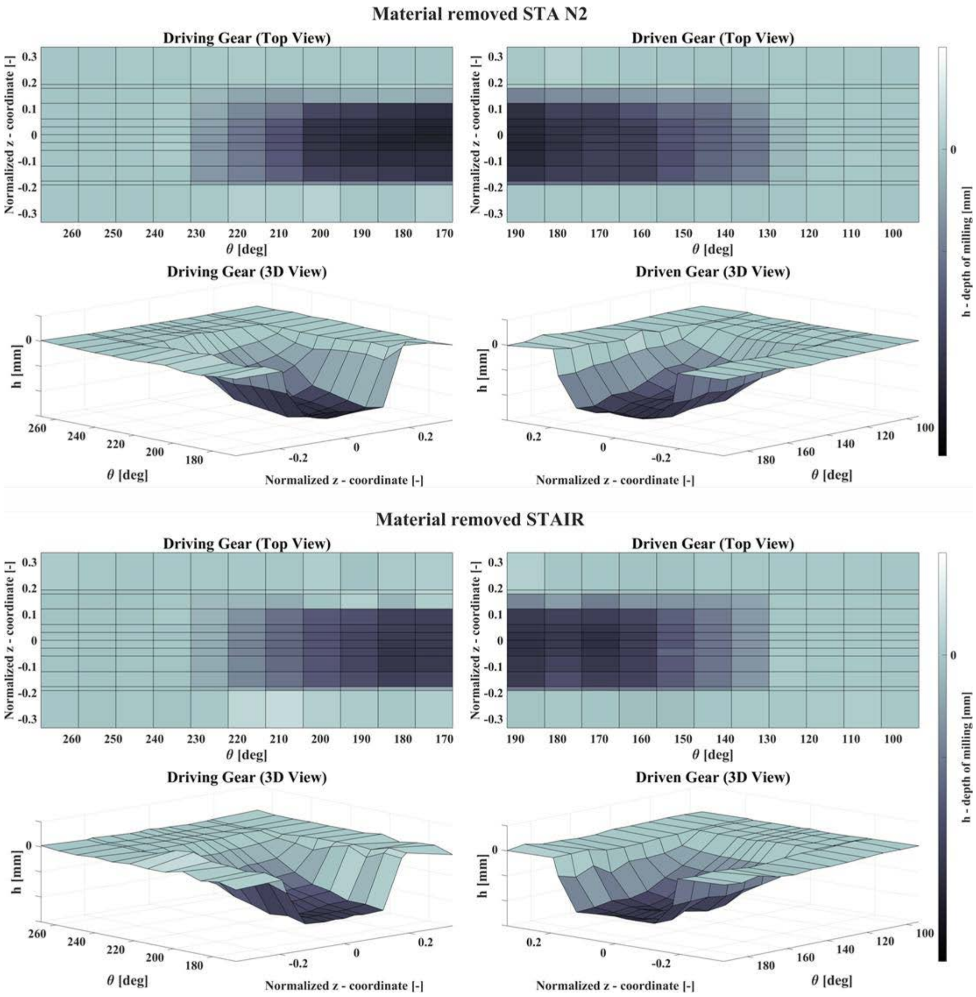

Figure 3. 6 - Top View and 3D view of the material removed on the suction side for the STA N2 and STAIR cycles

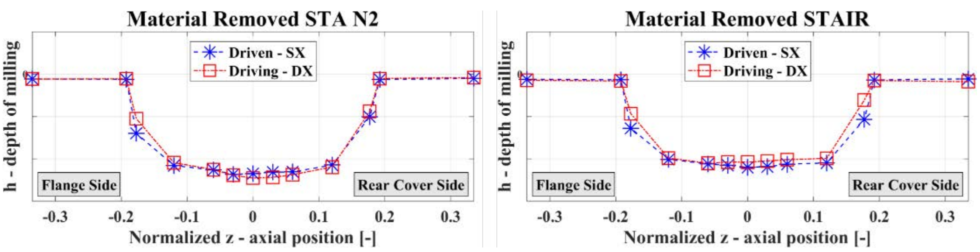

Figure 3. 7 - Milling line in the axial direction

Significant improvements in volumetric efficiency were observed with almost all the new cycles (Figure 3. 4), but the STA N2 with higher shaft speed and volume of material removed showed worsening performance. The pressure gradient or the run-in cycle seems to have an impact on the material removal. Varying the run-in cycles but maintaining constant p_S^{max} and t_S^3, the internal profile shape changes slightly. From the analysis of the removed volume, it is possible state the following: 1) under a fixed pressure gradient, as the run-in speed increases, the material removal on the driving and driven gears becomes comparable between the driving and the driven gears and a greater total volume of material is removed with a negative impact on the volumetric efficiency (cycle STA N2 compared to STA N1); 2) contrarily, with a fixed rotational speed, as the pressure gradient increases (reduction of the time cycle) the total removed material decreases impacting positively on the volumetric efficiency (cycles STAIR, New STA, 1STEP 1 and 3 compared to STA N1). The increase in volumetric efficiency (Figure 3. 4) is directly correlated with the reduction of the removed material volume in gears seats (as shown Table 3. 3), where a lower volume corresponds to a reduced milling height (as shown in Figure 3. 6 and Figure 3. 7). In conclusion, the combination of p_S^{max} and N defines the final internal profile shape [1] and the maximum depth of milling [2].

4. AI ALGORITHM: TORQUE PREDICTION

With the future goal of optimize the run-in cycle, a preliminary model based on AI algorithm has been developed. The use of an AI-based tool is motivated by the need to model a complex, non-linear and transient behaviour of an external gear pump, which is difficult to describe accurately using purely physics-based approaches. An EGP, equipped with sensors, generates data in the form of time series that represent the inputs and outputs for the model. For this activity, at this initial stage, the commercial software NeurEco® [7], with a specific dynamic template for processing time series data, has been used for the creation of a predictive model. The tool defines a neural network through a controlled topological enrichment process that uses parsimony to reach optimal accuracy [8]. The procedure starts from a minimal architecture that is progressively enriched by adding the most valuable neurons and connections as needed. This iterative expansion of the architecture allows the model to reach the global optimum for the problem. When no further enrichment improves the prediction, the process stops. This approach provides the model with the requested complexity. NeurEco® enforces a minimal model size, which eliminates overfitting by construction.

This commercial tool was used to develop a preliminary AI-based predictive model for the EGPs run-in cycle. The first application of the model was focused on predicting of the torque needed during the 1st and 6th run-in, having the delivery pressure profile as input. The analysis presented in this section refers to the cycles with the N1 speed. Considering that the 6th run-in was acquired only for one pump for each cycle type, the total data set available was composed of five continuous acquisitions (STA N1, STAIR, New STA, 1STEP 1 and 1STEP 3), while for the first run-in cycle all the five samples were available for each cycle.

Firstly, a dynamic physical model, called Model0, with the pressure profile as input, was built for predicting the 6th run-in (with no material removal). The model outputs are torque, which allows for estimating the hydromechanical efficiency, and the absorbed energy of the EGP. Three samples, STA N1, 1STEP 1 and New STA, were used for the training phase and the remaining two, STAIR and 1STEP 3, were used for the blind test phase. Figure 4. 1 shows the acquired (*exp.*) and predicted (*pre.*) torque for the 6th run-in 1STEP 3. The average error on the torque prediction was 0.93% and, on the energy (calculated using equation 2.1) was 0.68%. Despite the small training sample size, the model showed a very good capability in the prediction of the torque in the absence of material removal (in fact, during run-in 6th there is no interference between gear teeth and pump body). In the second phase, the pressure profile and the predicted torque by the Model0 were used as inputs to a second model for predicting the torque needed during the run-in with material removal. Thus, the Model0 output was used as input for the improved model, called Model1. The inputs for Model1 were the pressure profile, as per Model0, and the torque predicted by Model0. The results of Model1 are reported in Figure 4. 1 and compared to Model0 and the experimental curve. Even if the *pre.* curve (red dashed line) associated to run-in 1 does not capture the spikes and fluctuations of the experimental torque curve, the results of Model1 can predict the average value of the torque during the material removal of the run-in cycle with an average error of 5.87% and an error less than 0.11% on the required energy (lower than Model0 as expected). Model1, with respect to the Model0, was trained on a sample of fifteen acquisitions. Starting from the duty cycle (pressure profile), the combinate use of Model0 and Model1 (Figure 4. 2.a) allows for predicting with a small error the run-in torque, energy and hydromechanical efficiency. In the present work, the AI model represented by Figure 4. 2.a was tested for a unique pump displacement and for load cycles belonging to the families defined in Table 2. 1.

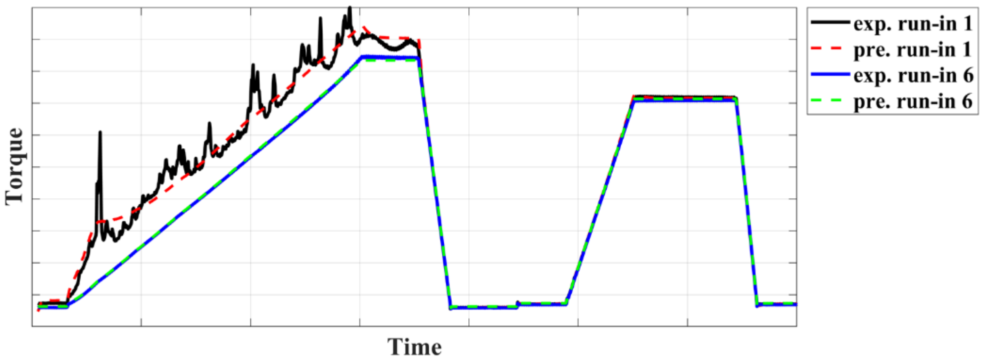

Figure 4. 1 – Experimental (exp.) and Predict (pre.) torque for the 1STEP 3 cycle

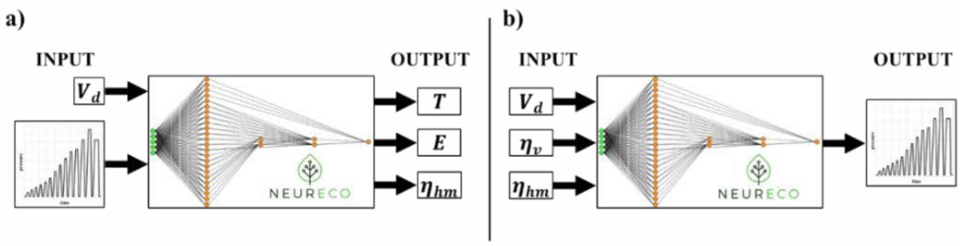

Figure 4. 2 – a) Actual predictive AI model; b) Desired predictive AI model

The present AI model represents a first step toward optimizing run-in cycles (as shown in the flowchart in Figure 4. 2.b); consequently, in future works, it will be tested on various pump displacements and duty cycles to better understand its behaviour far away the training conditions. As said, at the present, the model is not able to predict the gears seats profile, torque spikes and fluctuation (but can be considered negligible, having the purpose of optimizing the run-in cycle) and the volumetric efficiency. The last can be included by recording the flow rate during run-in cycle.

5. CONCLUSION

The paper presents a deep analysis focused on the run-in cycle of EGPs made thought an extended experimental investigation and the definition of a preliminary AI-based model. Thirty pumps were tested with six different types of run-in cycles, showing interesting results in terms of pump performance improvement and cost reduction. For all the pumps, the same maximum load (p_S^m) was set and the same shape of the internal body profile, with slight differences in the height of milling and in the total volume removed, was obtained. One interesting result is that the final profile shape of the driver gears seats results deeper and aligned with the driven gear when the run-in speed increases, keeping constant the maximum pressure, impacting negatively on the volumetric efficiency. Moreover, adopting new cycles with the same maximum pressure but reduced cycle time the final profile shape of gears seats changes slightly (Table 3. 3) and a minor height of milling is achieved with significantly impacts on the pump efficiency (Figure 3. 4). For the shorter cycles, it was experimentally verified that, the complete material removal requires a time at the maximum load greater than the reference cycle STA N1; spikes of torque appeared on the second and third run-in cycles. Thus, for future activities, a variable t_S^3 will be considered to find the minimum time necessary to have the finished internal profile. The adoption of a shorter cycles ensured a pump cost reduction of 1.74% and an increase in the testing capability until to 78% for the 1STEP 1 cycle. At the same time, the shorter cycles, in particular the 1STEP 3 and the STAIR, showed an increment of pumps performances thanks to a higher volumetric efficiency. The latter benefit was predominant at the low speeds and at the medium-low pressures; working conditions in which the percentage weight of the tip leakages is more relevant. In the STAIR, 1STEP 1 and 1STEP 3 cycles, the run-in phase did not include time intervals for depressurisation, in which the body surface milled by the gears could cool down and the material could be easily removed, and this could have affected the surface quality. In future works, a detailed analysis of the surface asperities in the wear zone will be provided. Therefore, optimising the run-in cycle can ensure economic benefits and improved pump performance. A preliminary AI model for the prediction of the run-in process variables (torque) was developed using the commercial tool NeurEco®. Despite the small size of the training sample, the model was able to predict the absorbed torque, with an error below 6% for the run-in 1 and below 1% for the run-in 6. In future activities, the prediction of other physical quantities, such as the flowrate (therefore volumetric efficiency) and the material removed.

6. APPENDIX

6.1. *Definition of $\delta_r^{av.}$ $\epsilon_{max}^{av.}$ and int*

The three quantities $\delta_r^{av.}$, $\epsilon_{max}^{av.}$ and int are defined as:

$\delta_r = r^{body} - r^{gear}$; $\delta_r^{av.} = \left(\delta_r^{driving} + \delta_r^{driven}\right)/2$ where r identifies a radius and δ a radial clearance.

$\epsilon_{max} = \left(r^{body} - r_{ex}^{thrust\ plate}\right) + (r_{in}^{thrust\ plate} - r^{shaft})$ where ex and in identify the external and internal radius. Considering the two pump sides, flange and rear cover, and the two gears, driven and driving is obtained $\epsilon_{max}^{av.} = (\epsilon_{max}^{driving-flange} + \epsilon_{max}^{driving-cover} + \epsilon_{max}^{driven-flange} + \epsilon_{max}^{driven-cover})/4$. Combining $\delta_r^{av.}$ and $\epsilon_{max}^{av.}$ the quantities int is defined as $int = \epsilon_{max}^{av.} - \delta_r^{av.}$. This last identifies the radius interference between the teeth of the gears and the pump body under the condition of max radial shift of the shaft ϵ_{max}.

6.2. Effective Energy Variation

The passage from equation (3. 1) to equation (3. 2) is possible under various simplifying assumptions.

Assuming that all the pumps with the same RB have the same hydromechanical efficiency, $\eta_{hm,j}^{STA\ N1} = \eta_{hm,j}^{STA\ N2} = \eta_{hm,j}^{STAIR} = \cdots = \eta_{hm,j}^{1STEP\ 3} = \eta_{hm,j}$ for $j = 1,2,\dots 5$, the equation. (3. 1) can be rewritten as:

$$\delta E_{i,j}^{eff} = \frac{\left(\frac{1}{\eta_{hm,j}}\right)\left[\left(E_{i,j}^{th} + \eta_{hm,j} * E_{i,j}^{eff-mill}\right) - \left(E_{STA\ N1,j}^{th} + \eta_{hm,j} * E_{STA\ N1,j}^{eff-mill}\right)\right]}{\left(\frac{1}{\eta_{hm,j}}\right)\left(E_{STA\ N1,j}^{th} + \eta_{hm,j} * E_{STA\ N1,j}^{eff-mill}\right)} * 100$$

Under the assumption that the energy required for the material remotion is the same for all the pumps tested (thirty), $E_{i,j}^{eff-mill} = E^{eff-mill} > 0$ for $j = 1,2,\dots 5$ and $i = \{STA\ N1, STA\ N2, STAIR, New\ STA, 1STEP\ 1, 1STEP\ 3\}$, the above equation becomes:

$$\delta E_{i,j}^{eff} = \frac{E_{i,j}^{th} - E_{STA\ N1,j}^{th}}{\left(E_{STA\ N1,j}^{th} + \eta_{hm,j} * E_{STA\ N1,j}^{eff-mill}\right)} * 100 = \delta E_i^{th} * \frac{E_{STA\ N1,j}^{th}}{\left(E_{STA\ N1,j}^{th} + \eta_{hm,j} * E^{eff-mill}\right)}$$

Defined A as:

$$A = \frac{E_{STA\ N1,j}^{th}}{\left(E_{STA\ N1,j}^{th} + \eta_{hm,j} * E^{eff-mill}\right)} < 1$$

The equation. (3. 2) is obtained. It is important to highlight that the assumption of a unique value of $E^{eff-mill}$ considers that for all the pumps there is the same amount of material removed. This hypothesis can be valid for two reasons: 1) All the run-in cycles have the same maximum pressure (defines the gears' inflection and shift towards the inlet); 2) The thirty pumps have been assembled, maintaining control of the variability of the radial clearances.

If $E_{i,j}^{eff-mill}$ is not constant the parameter B can be defined as:

$$B = \frac{E_{i,j}^{eff-mill} - E_{STA\ N1,j}^{eff-mill}}{\left(\frac{1}{\eta_{hm,j}}\right)\left(E_{STA\ N1,j}^{th} + \eta_{hm,j} * E_{STA\ N1,j}^{eff-mill}\right)} * 100$$

Using the parameters A and B the equation (3. 1) becomes the equation (3. 3). The sign of B depends by the relationship between $E_{i,j}^{eff-mill}$ and $E_{STA\ N1,j}^{eff-mill}$.

Acknowledgment and Data availability

The authors would like to thank ADAGOS, BSim Engineering, and Hydreco Hydraulics for their technical support. For confidential reasons, the data are not available.

References

[1] Dalpiaz, G.; Fernández, A.; Mucchi, E. Modeling run in process in external gear pumps. In Proceedings of the ASME 8th Biennial Conference on Engineering Systems Design and Analysis, Torino, Italy, 4–7 July 2006; pp. 927–936. DOI:10.1125/ESDA2006-95466

[2] M.Borghi, M. Milani, F. Paltrinieri, M. Guidetti. Influenza Del Rodaggio Sulle Condizioni Di Funzionamento Di Macchine Volumetriche Ad Ingranaggi Esterni. 56° Congresso Nazionale ATI.

[3] Osiński, P.; Bury, P.; Cieślicki, R. Optimizing the Break-in Process of High-Pressure Gear Pumps. In Advances in Hydraulic and Pneumatic Drives and Control 2020 (NSHP 2020), Poland; Stryczek, J., Warzynska, U., Eds.; Lecture Notes in Mechanical Engineering; Springer: Cham, Switzerland, 2020. DOI: 10.1007/978-3-030-59509-8_6.

[4] S.Manco, N. Nervegna, Simulation of an external gear pump and experimental verification, Proceedings of the JFPS International Symposium on Fluid Power, 1989(1), 147–160. doi:10.5739/isfp.1989.147.

[5] B. Peric; M. Engler; M. Schuler; P. Woias; Using Neural Networks as a Data-Driven Model to Predict the Behavior of External Gear Pumps; Processes 2024, 12(3), 526; https://doi.org/10.3390/pr12030526

[6] K. Lakshmanan, A. J Gil, F. Auricchio, F. Tessicini; A fault diagnosis methodology for an external gear pump with the use of Machine Learning classification algorithms: Support Vector Machine and Multilayer Perceptron. DOI: 10.17028/rd.lboro.12097668.v1.

[7] Neureco – AI and Digital Twin data-based for engineers | Bsim Engineering

[8] Bashtova, K., Causse, M., James, C., Masmoudi, F., Masmoudi, M., Turki, H., & Wolff, J. "Application of the topological gradient to parsimonious neural networks." Computational Sciences and Artificial Intelligence in Industry: New Digital Technologies for Solving Future Societal and Economical Challenges. Cham: Springer International Publishing, 2021. 47-61.

Biographies

Alfonso Rosario Apuzzo received the bachelor's degree in aerospace engineering from University of Naples Federico II in 2021, the master's degree in mechanical engineering from the University of Naples Federico II in 2024. In November 2024 started the PhD program born from the collaboration of the University of Sannio and the Duplomatic MS company. His research includes the study of the external gear pumps via numerical and experimental approaches.

Sara Bonati received her MSc degree in mechanical engineering from the University of Parma in 2016. At the same university, she carried out a research grant in 2016 concerning the development of lumped-parameter fluid dynamics models of positive displacement compressors. She has been working since 2017 in the field of Fluid Power, focusing on research and product development activities through CAE tools. She joined the Duplomatic Group in 2023 as R&D drive system engineer.

Dr. Emma Frosina is an Associate Professor in the Department of Engineering at the University of Sannio, Benevento. She received her M.S. degree in Mechanical Engineering from the University of Naples Federico II in 2012 and her Ph.D. degree in Mechanical Systems Engineering in 2016. She is the author of over 80 scientific papers published in peer-reviewed international journals and conference proceedings. Her research interests are in the field of fluid power, where she specializes in the modeling and optimization of components (machines, valves, etc.) using numerical approaches (both lumped parameter and three-dimensional CFD) and experimental testing.

Dr. Luca Riccò received his MSc degree in mechanical engineering in 2012 and his PhD in industrial engineering in 2015 from the University of Parma. After, he started his career in the field of fluid power with different R&D roles. Starting from July 2023 he leads the R&D drive system and global simulation team of the Duplomatic Group, a member of Daikin Group.